2nd IJERW on Hydraulic Structures. S. Pagliara (ed.) ©2008 Edizioni Plus. University of Pisa. Pisa. Italy - ISBN: 978-88-8492-568-8

in skimming flows

S. Felder & H. Chanson

Department of Engineering, University of Aberdeen, Scotland (Formerly research scholar in Civil Engineering, The University of Queensland, Brisbane QLD 4072, Australia), stefan.felder@web.de

Division of Civil Engineering, The University of Queensland, Brisbane QLD 4072, Australia, h.chanson@uq.edu.au

ABSTRACT**:** Stepped spillways are a form of flood release facility. Flows down stepped spillways are characterised by a high rate of energy dissipation. They are however characterised by complex turbulent processes. Physical experiments were conducted on a large-size stepped spillway model at the University of Queensland operating with large discharges: i.e., for a skimming flow regime. Extensive measurements were conducted to provide a better understanding of the interactions between mainstream turbulence, step cavity recirculation and free-surface aeration. The present study focused on the turbulence properties including turbulence intensity and integral turbulent scales. Downstream of the inception point of free-surface aeration, the distributions of turbulence intensities highlighted an alternation of vertical profiles every two step edges linked with some form of vortex shedding. The distributions of integral turbulent time and length scales were measured at several step edges for several discharges. The results highlighted the strong turbulence levels and turbulent dissipation in the intermediate flow region defined as $0.3 < C < 0.7$. This region within the bulk of the flow played an important role in terms of energy dissipation. The results demonstrated some characteristic maxima of integral turbulent scales and self-similar relationships between some characteristic dimensionless integral turbulent scales and the Reynolds number.

1 INTRODUCTION

For large flood events, a dam needs a flood release facility to prevent dam overtopping and the failure of the structure. The flood discharge structure must dissipate the kinetic energy of the flow to avoid damage to the river banks and to the dam wall. One type of flood release facility is the stepped spillway design. Its construction is compatible with simple and economic dam construction techniques such as RCC and gabions (Figure 1). A stepped spillway is characterised by a high rate energy dissipation which yields the construction of smaller and cheaper downstream stilling basins (CHANSON 2001).

The steps are large rough elements that cause a significant flow resistance and increase the flow aeration. This aeration is a characteristic feature of all stepped spillway flows and it is linked with the whitish colour of the air-water flow, commonly described as "white waters". In high-velocity flows on spillways, air entrainment occurs naturally and its effect on the flow properties must be taken into account. Basic air-water flow parameters include the air concentration, or void fraction C, and the equivalent clear water flow depth

$$d = \int_0^{Y_{90}} (1 - C) \times dy \quad (1)$$

where Y_{90} is the depth normal to the spillway surface where the air concentration C is 90% and y is the distance normal to the pseudo-bottom formed by the step edges (CAIN & WOOD 1981).

At the upstream end of the spillway, the flow is smooth and transparent. Above the steps, however, turbulence is generated and a boundary layer develops. When the outer edge of the boundary layer reaches the free-surface, free-surface aeration occurs. Downstream, some air is continuously entrained by the action of a multitude of irregular vortices acting next to the free-surface. It is well accepted that free-surface aeration occurs when the turbulence level is large enough to overcome surface tension (CHANSON 1997).

For relatively large discharges, the water flows down the stepped cascade as a coherent stream: i.e., the skimming flow (RAJARATNAM 1990, CHANSON 2001). The step edges form a pseudo-bottom over which the waters skim (Figure 2). Beneath the pseudo-bottom formed by the step edges, intense recirculating vortices develop.

Figure 1. Construction of the Meander dam (Aus.) on 27 February 2007 (Courtesy of the Tasmanian Rivers & Water Supply Commission) - Note the precast concrete steps to assist the RCC placement and the right abutment plinth construction


Figure 2. Skimming flow regime on the stepped spillway model of the present study, side view of experimental section (flow from left to right)

The cavity recirculation is maintained through the transmission of shear stress from the main stream flow, and a large proportion of the kinetic energy is dissipated in this process (CHANSON 1994, OHTSU et al. 2004).

High-velocity skimming flows above stepped spillways are however complicated and the physical flow mechanisms are not well known. The present study focused on some turbulence properties in air-water skimming flows above moderate slope stepped spillways. It is the purpose of this contribution to provide a better understanding of the complex interactions between mainstream turbulence, step cavity recirculation and free-surface aeration based upon physical experiments conducted in a large-size facility.

2 OUTLINE OF THE EXPERIMENTAL STUDY

New experiments were conducted at the University of Queensland, Brisbane (Australia) in a large-size stepped spillway model with a 1 m wide channel equipped with 20 flat steps with heights of 5 cm and lengths of 12.5 cm. The chute slope (21.8°) is typical of embankment dam slopes. The experiments were performed in the skimming flow regime with discharges per unit width q_w ranging from 0.044 to 0.173 m^2/s. Based upon a Froude similitude, the corresponding dimensionless discharge d_c/h was between 1.15 and 2.9, where d_c is the critical flow depth

$$d_c = \sqrt[3]{q_w^2/g}\,, \qquad (2)$$

with g the gravity acceleration and h the step height. The Reynolds numbers $\mathrm{Re} = \rho_w \times V \times D_H / \mu_w$ were between 1.74 10^5 and 6.89 10^5, where D_H is the hydraulic diameter, ρ_w is the water density, μ_w is the dynamic viscosity and V is the flow velocity. Table 1 summarises the experimental conditions.

q_w [m²/s]	d_c/h	Re	Instrumentation	Inception point
0.044	1.15	1.74×10^5	Two single-tip probes Double-tip probe	6 to 7
0.078	1.7	3.10×10^5	Double-tip probe	9 to 10
0.122	2.3	4.85×10^5	Two single-tip probes Double-tip probe	14 to 15
0.147	2.6	5.83×10^5	Double-tip probe	15 to 16
0.173	2.9	6.89×10^5	Two single-tip probes Double-tip probe	17 to 18

Table 1. Experimental flow conditions of the present study

Two types of phase detection intrusive probes (needle tip design) were used: either two identical single-tip conductivity probes with an inner electrode sensor size of 0.35 mm, or a double-tip conductivity probe with an inner electrode of 0.25 mm. These probes were designed to pierce the air bubbles and water droplets and the phase detection principle was based upon the different electrical resistivity of air and water (CHANSON & CAROSI 2007b). When an air bubble passed the probe-tip, the current between the electrodes stopped and the voltage decreased suddenly. Each sensor was sampled for 45 seconds with a sampling rate of 20 kHz yielding 900,000 data per probe sensor per sampling location.

The single-tip conductivity probes were used to measure the basic air-water flow properties. One probe, the reference probe, was positioned on the channel centreline (z = 0) the second probe sensor was located at the same longitudinal and normal co-ordinates (x, y), but was separated by a transverse distance Δz from the reference probe tip. The separation distance Δz was systematically varied from 3.6 mm to 60.3 mm (Figure 3). A signal

processing based on a single threshold technique yielded the void fraction, bubble count rate F and chord size distributions (TOOMBES 2002).

Figure 3. Two single-tip probes with transverse distance Δz = 8.5 mm

Further measurements were conducted with the double-tip conductivity probe at all step edges downstream of the inception point for all discharges. The probe consisted of two identical tips, the leading, reference tip, and the trailing tip seperated by a streamwise distance Δx of 7 mm. The successive detection of every bubble by each probe sensor was highly improbable, because of the turbulent flow characteristic. Indeed the fluid motion in this turbulent flow was characterised as an irregular condition flow in which the various quantities showed a random variation with time and space coordinates.

Therefore a cross-correlation technique was used to determinate the advection parameters (CROWE et al 1998, CHANSON 2002). Auto- and cross-correlation analyses of the simultaneously sampled raw signals of the two probe sensors yielded the interfacial velocities V, which were the time-averaged velocities, and some information about the velocity fluctuations at all measured locations above channel bed y. CHANSON & TOOMBES (2002) derived an expression for the interfacial velocity fluctuation, and the turbulence intensities Tu were calculated as:

$$Tu = 0.851 \times \frac{\sqrt{{\tau_{0.5}}^2 - {T_{0.5}}^2}}{T} \quad (3)$$

where the travel time T is the time for which the cross-correlation function is maximum, $\tau_{0.5}$ is the time scale for which the cross-correlation function is half of its maximum value such as: $R_{xz}(T+\tau_{0.5}) = 0.5 \times R_{xz}(T)$, R_{xz} is the normalised cross-correlation function, and $T_{0.5}$ is the characteristic time for which the normalised auto-correlation function equals: $R_{xx}(T_{0.5}) = 0.5$.

Following MURZYN et al. (2006) and CHANSON (2007) on hydraulic jumps, and CHANSON & CAROSI (2007a,2007b) on a stepped spillway model, integral turbulent time and length scale measurements were performed with the array of two single-tip conductivity probes. Some typical raw signal outputs of two simultaneously sampled single-tip sensors are shown in Figure 4 for the same discharge and at the same location but with a transverse separation distances Δz of 3.7 mm and 29.9 mm respectively. In Figure 4, the upper plot (Δz = 3.7 mm) shows clearly some similarities between the two signals while, in the lower plot (Δz = 29.9 mm), there is little correlation. A comparison of the two plots suggests a decrease in signal correlation with increasing probe distance. Figure 4 implies the existence of large transverse flow structures with transverse scales of less than 30 mm. The large eddies are responsible for the advection of the air bubbles and air-water packets.

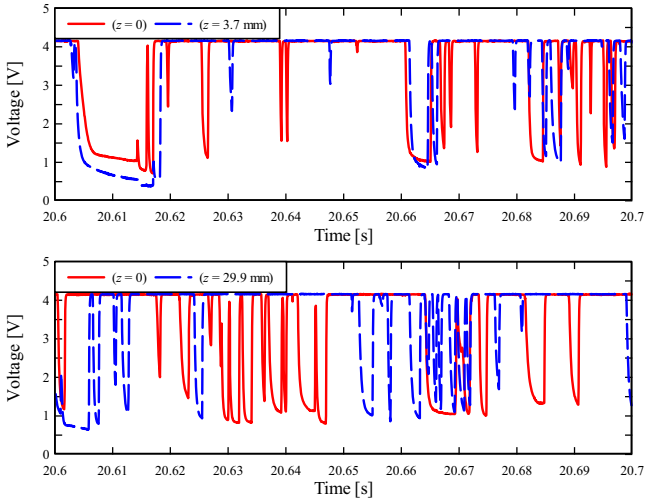

Figure 4. Raw signals of two single-tip conductivity probes with transverse distance Δz, d_c/h = 1.15, Re = 1.7×10^5, step 18, y = 0.022 m, C = 0.25, F = 150 Hz: upper plot: $(R_{xz})_{max}$ = 0.522, Δz = 3.7 mm; lower plot: $(R_{xz})_{max}$ = 0.099, Δz = 29.9 mm

Based upon the technique of CHANSON & CAROSI (2007a), the auto- and cross-correlation analyses were performed on the output signals of the two single-tip conductivity probes. The results yielded the auto- and cross-correlation functions R_{xx} and R_{xz}, and the maximum correlation coefficient $(R_{xz})_{max}$. The integration of the correlation function between the maximum correlation and the first zero-crossing yielded the auto- and cross-correlation integral time scales defined as:

$$T_{xx} = \int_{\tau=0}^{\tau=\tau(R_{xx}=0)} R_{xx}(\tau) \times d\tau \quad (4)$$

$$T_{xz} = \int_{\tau=\tau(R_{xz}=(R_{xz})_{max})}^{\tau=\tau(R_{xz}=0)} R_{xz}(\tau) \times d\tau \quad (5)$$

where τ is the time lag and R_{xz} is the normalised cross-correlation function between the two probe output signals. T_{xx} is the auto-correlation integral time scale which represents the longitudinal air-water flow structure. T_{xz} characterises the transverse

vortices advecting the air-water flow structure and is a function of the probe separation distance.
The integration of $(R_{xz})_{max}$, between the maximum correlation and the maximum separation for which the correlation tended to zero, yielded the transverse integral turbulent length scale:

$$L_{xz} = \int_{z=0}^{z=z((R_{xz})_{max}=0)} (R_{xz})_{max} \times dz \quad (6)$$

and the turbulent integral time scale:

$$T_{int} = \frac{\int_{z=0}^{z=z((R_{xz})_{max}=0)} (R_{xz})_{max} \times T_{xz} \times dz}{L_{xz}} \quad (7)$$

Some streamwise integral turbulent length scales L_{xx} were also calculated. The calculation was based upon Taylor's hypothesis of frozen turbulence:

$$L_{xx} = V \times T_{xx} \quad (8)$$

Equation (8) yielded a characteristic longitudinal size of the large advection vortices.

3 EXPERIMENTAL RESULTS OF THE PRESENT STUDY

The new experiments gave an extensive data set for a characterisation of the highly complex skimming flows. Basic air-water flow properties included the distributions of void fraction, bubble count rate and interfacial velocity for all experimental runs. The data yielded air-water flow properties that were close to and consistent with earlier studies on stepped spillways (GONZALEZ and CHANSON 2004, CHANSON & CAROSI 2007a).
Figure 5 illustrates some typical dimensionless distributions of void fraction and interfacial velocity at one step edge. The void fraction distributions compared well with the advective diffusion equation for air bubbles, first derived by CHANSON & TOOMBES (2002). The interfacial velocity distributions were best fitted by a 1/10 power-law function for $y/Y_{90} < 1$ and by a uniform profile for $y/Y_{90} > 1$ (GONZALEZ 2005). These theoretical approximations are shown in Figure 5.
The complete air-water properties and the whole data set of the present study are available in FELDER & CHANSON (2008). In the present paper, the experimental observations of some turbulence properties are presented.

3.1 *Turbulence intensity distributions*

With the double-tip conductivity probe, measurements were performed at all steps downstream of the inception point of air entrainment. The turbulence intensities were calculated for a wide range of discharges.

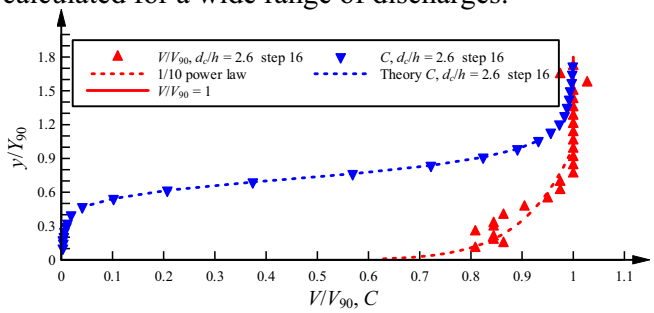

Figure 5. Dimensionless distributions of void fraction C and interfacial velocity V/V_{90} – comparison with theories, d_c/h = 2.6, Re = 5.8×10^5; double-tip probe

Note that Equation (3) was not strictly comparable to the turbulence intensity in mono-phase flows because the velocity determination in air-water flows is spatially-averaged. However the distributions of the interfacial velocity fluctuations provided both qualitative and quantitative information on the turbulence field in the two-phase flow mixture. Typical turbulence intensity distributions are illustrated in Figure 6 as functions of the dimensionless distance normal to the pseudo-bottom y/Y_{90} for a flow rate at several successive step edges. The void fraction distribution for a step edge is also added for completeness.
Two different shapes for the turbulence intensity Tu distributions were observed consistently. The first type is illustrated in Figure 6 with dotted lines. For that shape, the turbulence maxima were observed for void fractions between 0.4 and 0.6, while the second shape shows distributions with lesser maximum turbulence values at locations corresponding to smaller void fractions. Both type of turbulent intensity profiles alternated every two steps. The alternation was believed to be caused by vortex shedding downstream of the step edge and the interactions with the next step edge. The turbulence intensity distributions for all experiments showed some maximum values up to 150% in the intermediate flow region ($0.3 < C < 0.7$), and the findings were consistent with earlier observations in stepped spillway models (e.g. CHANSON & TOOMBES 2002, GONZALEZ 2005, CHANSON & CAROSI 2007a).
The intermediate region ($0.3 < C < 0.7$) was located in the bulk of the flow with comparable air and water volume ratios. There, collisions, deformations and reformations of water droplets and air bubbles were very energetic processes that caused significant

energy dissipation and were linked with high turbulence levels. In contrast, close to the pseudo-bottom in the bubbly flow region ($C < 0.1$), and in

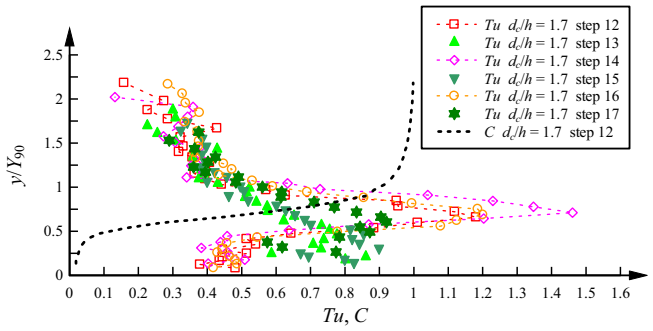

Figure 6. Dimensionless distributions of void fraction C and turbulence intensity Tu - illustration of two shape types, d_c/h = 1.7, Re = 3.1×10^5; double-tip probe

the spray region ($C > 0.9$), the turbulence level Tu was about 25 to 50%.The turbulence intensity distributions in two-phase skimming flows differed significantly from observations in mono-phase flow upstream of the inception point by AMADOR et al. (2006). These measurements had similar shapes to those observed in open channel flows (e.g. NEZU & NAZAGAWA 1993), but with larger intensities close to 100% near the pseudo-bottom. CHANSON & TOOMBES (2002) explained the significant increase in turbulence levels in two-phase flows on stepped spillways by the interactions between entrained air bubbles and turbulent structures. Large amounts of air entrained downstream of the inception point yielded strong turbulence interactions between air bubbles and water droplets in the air-water flow region of $0.05 < C < 0.95$. These dynamic processes seemed to be linked with large air-water velocity fluctuations and high turbulence intensities.

The relationship between the amount of entrained air and the turbulence levels is illustrated in Figure 7, where Tu is presented as a function of the dimensionless bubble count rate $F\times d_c/V_c$, where V_c is the critical velocity. Following CHANSON & TOOMBES (2002), this relationship was correlated by a power law

$$Tu = 0.25 + a\times\left(\frac{F\times d_c}{V_c}\right)^b \quad (9)$$

where a is a proportionality constant and b is a constant which expresses the rate of increase in turbulence level as a function of the bubble count rate. Equation (9) reflects a monotonic increase of Tu with increasing bubble count rate. A bubble count rate of 0 yields Tu = 25% that is close to measurements in mono-phase flows.

The present data set identified an alternate trend of the exponent b in Equation (9) every two step edges, with values larger and smaller than 1. These alternations are illustrated with trend-lines in Figure 7 and they correlate well with the two observed shape types shown in Figure 6. For $b < 1$, the increase of Tu with increasing bubble count rate is smaller than for the case $b > 1$.

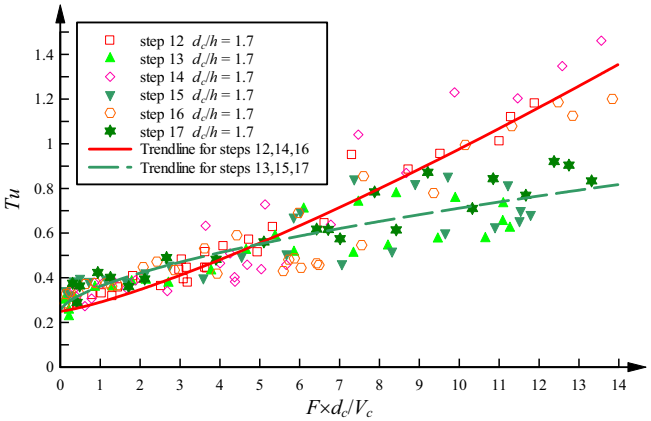

Figure 7. Relationship between turbulence intensity and dimensionless bubble count rate; trendlines of two steps alternations; d_c/h = 1.7, Re = 3.1×10^5; double-tip probe

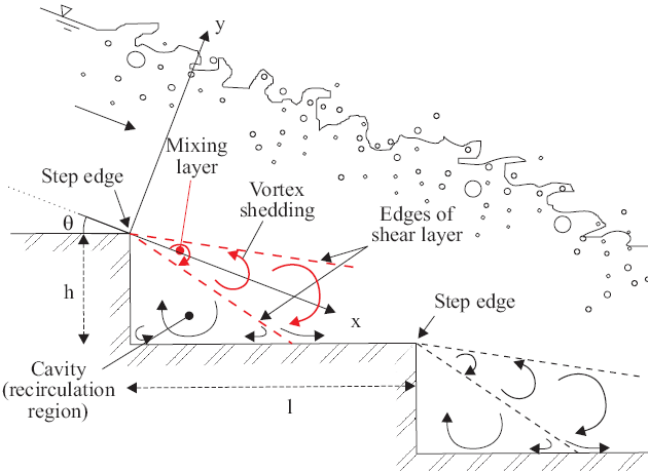

Figure 8. Sketch of cavity recirculation, vortex shedding and shear layer in a skimming flow above a step cavity

The present findings confirmed a monotonic relationship between bubble count rate and turbulence intensity, but highlighted two trends. The alternating trend every two step edges seemed to be linked with a characteristic seesaw pattern observed for several basic air-water flow properties in skimming flows on stepped spillways (e.g. YASUDA & CHANSON 2003, THORWARTH & KÖNGETER 2006, FELDER & CHANSON 2008). The alternation was believed to result from the interactions between cavity recirculation, main stream turbulence and free-surface aeration. At each step edge, a shear layer develops and causes some momentum transfer between main stream flow and the cavities (Fig. 8). Behind each step edge, vortices develop in the wake of the step edge associated with an advection of vorticity (GONZALEZ & CHANSON 2004). The shear layer and the vortices

impact on the downstream step flow and interfere with the physical process at the next step edge. The interactions between the shear layer and the adjacent step edge might cause the illustrated alternation (Fig. 6 & 7).

3.2 *Integral turbulent length and time scales*

Extensive measurements were conducted with an array of two identical single-tip conductivity probes and the data processing yielded the distributions of integral turbulent time and length scales at five step edges and for three discharges.

The distributions of integral turbulent scales had characteristic shapes that were typical for most measurements and similar to the earlier results of CHANSON & CAROSI (2007a). Figure 9 illustrates typical distributions of transverse integral turbulent length and time scales L_{xz} and T_{int} respectively and of the streamwise advection integral turbulent length scale L_{xx}. All integral scale distributions are illustrated in dimensionless terms as a function of y/Y_{90}. For completeness, the void fraction distribution is shown.

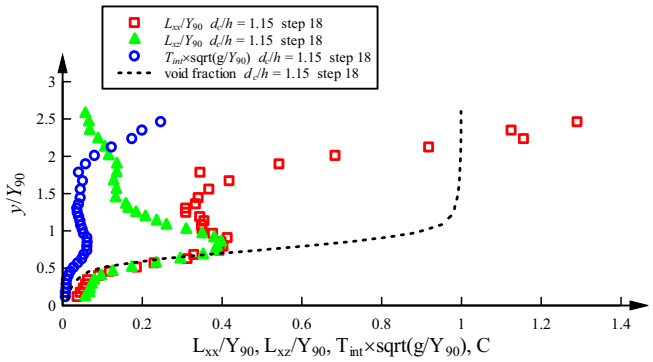

Figure 9. Dimensionless distributions of integral turbulent length L_{xz}/Y_{90} and time $T_{int}\times\sqrt{g/Y_{90}}$ scales and advection integral scales L_{xx}/Y_{90}; d_c/h = 1.15, Re = 1.74×10^5, step 18; two single-tip probes; void fraction distribution added

Firstly, for $0 \le C \le 0.97$ the distributions of T_{int}, L_{xx} and L_{xz} showed shapes with maximum values approximately in the intermediate flow region for $0.5 \le C \le 0.7$ (Fig. 9). For very small void fractions the distributions tended to zero. Secondly, a marked change in the distributions of T_{int} and L_{xz} was seen for $C > 0.97$. These results were consistent with the earlier findings of CHANSON & CAROSI (2007a). The results highlighted an upper spray region for $C > 0.95$ where the ejected spray did not interact with the rest of the flow. Thirdly, the shapes of transverse integral turbulent length scales L_{xz} and of advection turbulent length scales L_{xx} showed similar shapes for $C \le 0.95$. For $C > 0.95$ the distributions of L_{xx} and L_{xz} showed some significant deviations. These deviations tended to support the observations of the difference of the upper spray region from the rest of the flow.

The present observations identified also some characteristic maxima of transverse integral turbulent length and time scales, and of streamwise advection integral turbulent scales. Table 2 summarises the characteristic maximum values and they are compared with the data of CHANSON & CAROSI (2007a) [GH_06] obtained with 0.10 m high steps and the same bed slope (θ = 21.8°). In Table 2, the median values are also shown. Altogether, the integral turbulent length and time scale and advection turbulent length scale data were documented for seven step edges. Overall, for a stepped spillway model with a slope of 21.8°, the median values of the dimensional characteristic maximum scales were: $(L_{xx})_{max}$ = 14.1 mm, $(L_{xz})_{max}$ = 13.4 mm and $(T_{int})_{max}$ = 2.7 ms.

	Median	Present study (h = 0.05 m)					GH_06 (h = 0.1 m)	
d_c/h		1.15	1.15	2.3	2.3	2.9	1.15	1.45
Step		10	18	17	20	20	10	10
Y_{90} [mm]	69.2	33.4	35.4	69.2	85.9	97.8	59.8	73.5
$(L_{xx})_{max}$ [mm]	14.1	10.1	14.6	14.1	11.2	12.9	15.7	18.3
$(L_{xz})_{max}$ [mm]	13.4	9.3	14.1	15.2	10.9	12.6	13.4	16.9
$(T_{int})_{max}$ [ms]	2.7	2.6	3.8	2.7	2.3	2.3	3.7	3.5
$(L_{xx})_{max}/d_c$	0.127	0.176	0.255	0.123	0.097	0.089	0.137	0.127
$(L_{xz})_{max}/d_c$	0.117	0.161	0.245	0.133	0.096	0.087	0.116	0.117
$T_{int}\sqrt{g/d_c}$	0.029	0.034	0.049	0.025	0.021	0.019	0.034	0.029

Table 2. Presentation of characteristic advection length scales $(L_{xx})_{max}$, transverse integral turbulent time and length scales $(T_{int})_{max}$ and $(L_{xz})_{max}$ of the present study and of CHANSON & CAROSI (2007a) [GH_06]; (Note: $(L_{xx})_{max}$ and $(T_{int})_{max}$ valid for $0 \le C \le 0.97$)

The present observations confirmed the dimensionless relationships between integral turbulent scales and void fraction first proposed by CHANSON & CAROSI (2007a). For the combined data sets of both studies the self-similar relationships were best correlated by skewed parabolic laws:

$$\frac{L_{xz}}{(L_{xz})_{max}} = 1.58\times C^{0.48}(1-C)^{0.27} \qquad 0 < C < 1 \quad (10)$$

$$\frac{T_{int}}{(T_{int})_{max}} = 1.41\times C^{0.38}(1-C)^{0.23} \qquad 0 < C < 0.97 \quad (11)$$

$$\frac{L_{xx}}{(L_{xx})_{max}} = 1.46\times C^{0.40}(1-C)^{0.26} \qquad 0 < C < 0.97 \quad (12)$$

The self-similarity relationships are illustrated in Figure 10 for one step edge. Equations (10) to (12) correlated reasonably well with the data for all distributions. In the upper spray region, the

distributions of L_{xx} and T_{int} increased sharply due to the difference in the upper spray region.

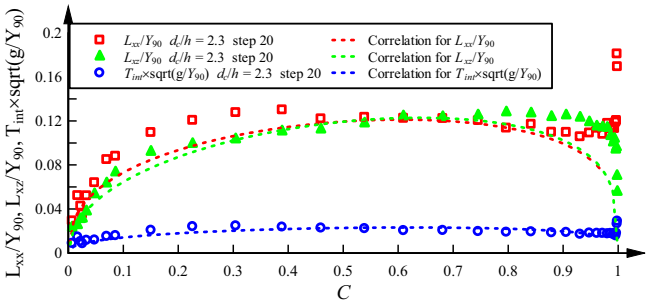

Figure 10. Dimensionless relationship between integral turbulent length L_{xz}/Y_{90} and time T_{int}×sqrt(g/Y_{90}) scales and advection integral scales L_{xx}/Y_{90} and void fraction C; d_c/h = 2.3, Re = 4.85×10^5, step 20; two single-tip probes

3.3 *Discussion*

A comparison of the turbulence intensities Tu and transverse integral turbulent length scales L_{xz} was performed to identify similarities between turbulence properties. These similarities might identify the most significant flow regions for turbulence processes in skimming flows. The comparison was conducted on the transverse integral turbulent length scales since the calculations of both L_{xz} and Tu were based upon the cross-correlation analyses of the raw signals.

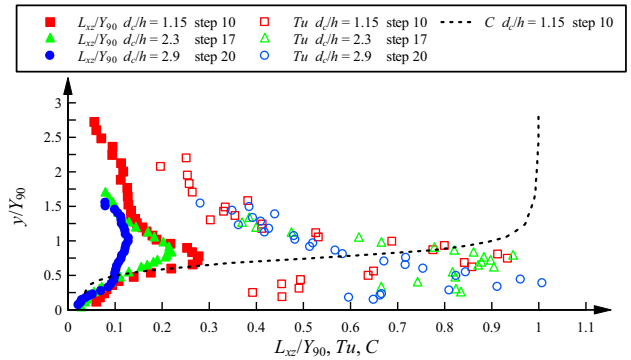

Figure 11: Comparison of transverse integral turbulent length scales L_{xz}/Y_{90} and turbulence intensity Tu for d_c/h = 1.15, 2.3, 2.9 at respectively three steps downstream of the inception point; void fraction distribution added

In Figure 11, some dimensionless distributions of turbulence level Tu and of integral turbulent length scale L_{xz}/Y_{90} are presented as functions of y/Y_{90} for several discharges. In each case, the data were collected at three step cavities downstream of the inception point. The void fraction distribution for one flow rate is shown for completeness.

All distributions showed some characteristic shapes with local maxima in the intermediate flow region for 0.3 < C < 0.7. They further showed that the maxima in L_{xz} and Tu occured for almost identical void fraction. In the intermediate flow region, both the largest advecting vortices and largest turbulence intensities were observed. That is, this region played a significant role for the development of large eddies and for turbulent kinetic energy dissipation.

Figure 11 highlights further a decrease of dimensionless integral turbulent length scales L_{xz}/Y_{90} with increasing discharge and interfacial velocity. Figure 12 reflects the trend for several discharges at respectively three steps downstream of the inception point in terms of the characteristic maxima of transverse integral turbulent time $(T_{\text{int}})_{\max} \times \sqrt{(g/d_c)}$ and length $(L_{xz})_{\max}/d_c$ scales and streamwise advection turbulent length scale $(L_{xx})_{\max}/d_c$ decreased with increasing Reynolds number Re. An increase in Reynolds number corresponds to an increase of discharge.

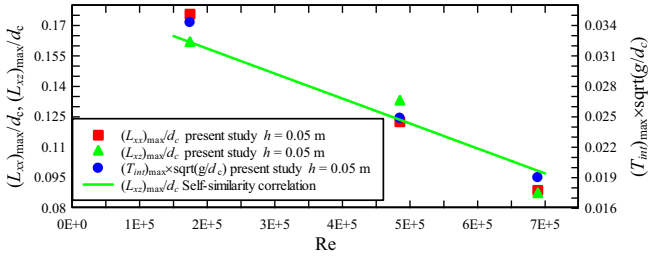

Figure 12: Dimensionless relationship between characteristic integral turbulent length $(L_{xz})_{\max}/d_c$ and time $(T_{int})_{\max}$×sqrt(g/d_c) scales and characteristic advection turbulent scales $(L_{xx})_{\max}/d_c$ and Reynolds number Re; h = 0.05; three steps downstream of inception point; two single-tip probes

For the present study, the dimensionless relationship between flow Reynolds number and integral turbulent time and length scales at three steps downstream of the inception point were best correlated by:

$$\frac{(L_{xx})_{\max}}{d_c} = 0.20 - 1.69\times10^{-7} \times \text{Re} \qquad (13)$$

$$\frac{(L_{xz})_{\max}}{d_c} = 0.18 - 1.23\times10^{-7} \times \text{Re} \qquad (14)$$

$$(T_{\text{int}})_{\max} \times \sqrt{(g/d_c)} = 0.04 - 2.98\times10^{-8} \times \text{Re} \qquad (15)$$

These self-similar relationships are valid for Reynolds numbers of almost one magnitude between 1.7×10^5 and 6.9×10^5. They are shown in Figure 12 and the results seemed independent of geometric scaling. An extrapolation at larger Reynolds numbers and for prototype conditions might to be possible.

4 CONCLUSIONS

An experimental study was conducted on a stepped spillway model for a broad range of discharges in

turbulent skimming flows to gain some information on the turbulence properties. The turbulence intensities were measured with a double-tip conductivity probe. The results showed an alternation of two different vertical profiles. This alternation seemed to be caused by complex interactions between recirculation motion in the cavities and the turbulent main stream flow, as well as interactions with the free-surface and interactions between flow processes in different flow regions.

With an array of two single-tip probes, transverse integral turbulent time and length scales were measured at several step edges. The observations of the integral turbulent scale distributions confirmed the earlier findings of CHANSON & CAROSI (2007a) highlighting a major difference between the upper spray region and the rest of the flow. The data set yielded some characteristic dimensional and dimensionless maxima values of the integral turbulent scales and some self-similar relationships that seemed independent of the geometric scaling. Furthermore a linear self-similarity between dimensionless integral turbulent scales and the Reynolds number was observed at respectively three steps downstream of the inception point.

A comparison between the distributions of turbulence intensities and transverse integral turbulent length scales was performed and showed some similarity. The largest turbulence intensities and the largest integral turbulent scales were observed in the bulk of the flow. In that intermediate region ($0.3 < C < 0.7$), large amounts of energy were dissipated by a combination of mechanisms, including air bubble entrainment, droplet generation and ejection, and particle break-up.

5 REFERENCES

Amador, A., Sanchez-Juny, M. & Dolz, J. 2006. Characterization of the Nonaerated Flow Region in a Stepped Spillway by PIV. *Journal of Fluids Engineering*, ASME, Vol. 128, No. 6, pp. 1266-1273.

Cain, P. & Wood, I.R. 1981. Measurements of Self-aerated Flow on Spillways. *Journal of Hydraulic Division*, ASCE, Vol. 107, HY11, pp. 1425-1444.

Chanson, H. 1994. Hydraulics of Skimming Flows over Stepped Channels and Spillways. *Journal of Hydraulic Research*, Vol. 32, No. 3, pp. 445-460.

Chanson, H. 1997. Air Bubble Entrainment in Free-Surface Turbulent Shear Flows. *Academic Press*, London, UK, 401 pages.

Chanson, H. 2001. The Hydraulics of Stepped Chutes and Spillways. *Balkema,* Lisse, The Netherlands, 418 pages.

Chanson, H. 2002. Air-Water Flow Measurements with Intrusive Phase-Detection Probes. Can we Improve their Interpretation? *Journal of Hydraulic Engineering*, ASCE, Vol. 128, No. 3, pp. 252-255.

Chanson, H. 2007. Bubbly flow structure in hydraulic jump. *European Journal of Mechanics B/Fluids*, Vol. 26, pp. 367-384.

Chanson, H. & Carosi, G. 2007a. Turbulent Time and Length Scale Measurements in High-Velocity Open Channel Flows. *Experiments in Fluids*, Vol. 42, No. 3, pp. 385-401 (DOI 10.1007/s00348-006-0246-2).

Chanson, H., & Carosi, G. 2007b. Advanced Post-Processing and Correlation Analyses in High-Velocity Air-Water Flows. *Environmental Fluid Mechanics*, Vol. 7, No. 6, pp. 495-508 (DOI 10.1007/s10652-007-9038-3).

Chanson, H. & Toombes, L. 2002. Air-Water Flows down Stepped chutes: Turbulence and Flow Structure Observations. *International Journal of Multiphase Flow*, Vol. 28, No. 11, pp. 1737-1761.

Crowe, C., Sommerfield, M., & Tsuji, Y. 1998. Multiphase Flows with Droplets and Particles. *CRC Press*, Boca Raton, USA, 471 pages.

Felder, S. & Chanson, H. 2008. Turbulence and Turbulent Length and Time Scales in Skimming Flows on a Stepped Spillway. Dynamic Similarity, Physical Modelling and Scale Effects. *Report No. CH64/07*, Division of Civil Engineering, The University of Queensland, Brisbane, Australia, 217 pages.

Gonzalez, C.A. 2005. An Experimental Study of Free-Surface Aeration on Embankment Stepped Chutes. *Ph.D. thesis*, Division of Civil Engineering, The University of Queensland, Brisbane, Australia, 240 pages.

Gonzalez, C.A. & Chanson, H. 2004. Interactions between Cavity Flow and Main Stream Skimming Flows: an Experimental Study. *Canadian Journal of Civil Engineering*, Vol. 31, No. 1, pp. 33-44.

Murzyn, F., Mouaze, D. & Chaplin, J.R. 2006. Flow visualisation and free surface length scale measurements in a horizontal jet beneath a free surface. *Experimental Thermal and Fluid Science*, Vol. 30, pp. 703-710.

Nezu, I. & Nakagawa, H. 1993. Turbulence in Open-Channel Flows. IAHR Monograph, IAHR Fluid Mechanics Section, *Balkema Publ.*, Rotterdam, The Netherlands, 281 pages.

Ohtsu, I., Yasuda, Y. & Takahashi, M. 2004. Flow Characteristics of Skimming Flows in Stepped Channels. *Journal of Hydraulic Engineering*, ASCE, Vol. 130, No. 9, pp. 860-869.

Rajaratnam, N. 1990. Skimming Flow in Stepped Spillways. *Journal of Hydraulic Engineering*, ASCE, Vol. 116, No. 4, pp. 587-591.

Thorwarth, J. & Köngeter, J. 2006. Physical Model Tests on a Stepped Chute with Pooled Steps. Investigations of Flow Resistance and Flow Instabilities. *Proc. Intl Symp. on Hydraulic Structures*, IAHR, Ciudad Guayana, Venezuela, pp. 477-486.

Toombes, L. 2002. Experimental Study of Air-Water Flow Properties on Low-Gradient Stepped Cascades. *Ph.D. thesis*, Division of Civil Engineering, The University of Queensland, Brisbane, Australia.

Yasuda, Y. & Chanson, H. 2003. Micro- and Macro-scopic Study of Two-Phase Flow on a Stepped Chute. *Proc. 30th IAHR Biennial Congress*, Thessaloniki, Greece, J. Ganoulis and P. Prinos Ed., Vol. D, pp. 695-702.